Design and Experimental Implementation of a New Robust Observer-based Nonlinear Controller for DC-DC Buck Converters

Samir ABDELMALEK[1*], Ali DALI[2], Azzeddine BAKDI[3], Maamar BETTAYEB[4]

[1]Faculty of Technology, Department of Electrical Engineering, University of Yahia Fares Medea, Algeria;
Email: s.abdelmalek.dz@gmail.com

[2] Centre de Développement des Energies Renouvelables, CDER, BP 62 Route de l'Observatoire, Bouzaréah, Alger, 16340, Algérie.
Email: a.dali@cder.dz

[3]Department of Mathematics, University of Oslo, 0851 Oslo, Norway.
Email: bkdaznsun@gmail.com

[4]Department of Electrical Engineering, University of Sharjah, United Arab Emirates, and Center of Excellence in Intelligent Engineering Systems (CEIES), King Abdulaziz, University, Jeddah, KSA.
Email: maamar@sharjah.ac.ae

[*]Corresponding author

E-mail: s.abdelmalek.dz@gmail.com

Abstract:

This paper considers the problem of DC-DC buck converter control for Maximum Power Point (MPP) tracking in renewable energy systems. A new nonlinear robust controller is proposed for fast and robust output voltage tracking in the DC bus of the power source. A novel composite sliding mode controller is developed with a nonlinear state observer design for current estimation. Parameters of the overall approach are tuned using Particle Swarm Optimization (PSO) algorithm with an objective to ensure a good balance between fast transients, robustness, and dynamic performance in practical implementations. This novel cost-efficient strategy accounts for the switched and nonlinear aspects of the problem in addition to disturbances. Stability of the closed-loop system is analyzed through Lyapunov stability theory. Moreover, comparative simulation tests and experimental results from multiple scenarios show significant trajectory-tracking improvements in terms of faster convergence with short transients and effective disturbance rejection performance compared to the optimally tuned Proportional Integral (PI) controller that is widely adopted in industrial applications.

Keywords—Robust nonlinear controller, nonlinear observer, PSO Algorithm, voltage tracking, DC-DC converter, Lyapunov theory, dSPACE 1103 platform.

Nomenclature

$\boldsymbol{\alpha}$	The switching control signal
$\boldsymbol{r_L}$	The inductor resistance (ohm)
$\boldsymbol{u}$	The PWM duty cycle
$\boldsymbol{V_c}$	The input DC-DC converter voltage (V)
$\boldsymbol{\hat{V}_c}$	The observer voltage (V)
$\boldsymbol{V_{dc}}$	The DC link voltage (V)
$\boldsymbol{V_{ref}}$	The reference voltage (V)
$\boldsymbol{\tilde{z}_1, \tilde{z}_2}$	The observer tracking errors
$\boldsymbol{C}$	The DC-DC converter capacitance (F)
$\boldsymbol{e_1, e_2, e_3}$	The tracking errors
$\boldsymbol{I_d}$	The input DC-DC converter current (A)
$\boldsymbol{\hat{I}_L}$	The observer inductance (A)
$\boldsymbol{I_{L_{ref}}}$	The inductor current reference (A)
$\boldsymbol{k_1}$	Parameter of the proposed observer
$\boldsymbol{K_p, K_i}$	Parameters of the MPPT controller
$\boldsymbol{L}$	The DC-DC converter inductance (H)

$\boldsymbol{\lambda_1, \lambda_2, \lambda_3, \lambda_4}$ Parameters of the proposed controller

Abbreviations

IAE	Integral Absolute-value of the Error
MPP	Maximum Power Point
MPPT	Maximum Power Point tracking
PI	Proportional Integral
PWM	Pulse Wave Modulation
PSO	Particle Swarm Optimization
RESs	Renewable Energy Sources

1. Introduction

The significant growth in energy demand and environmental issues has forced many countries around the globe to adopt clean energy sources [1]. Renewable energy sources (RES) are sustainable alternatives to deal with the increasing energy demand in our daily life. Electrical energy production from renewable clean sources is becoming a major revolution [1-2]. Recently, the increasing developments towards clean energy provide efficient solution for reducing the dependence on fossil fuels. Consequently, the integration of small wind power generators, solar energy generators and storage systems to the grid called 'microgrid system' consists one of the promising solutions which have drawn the attention of many researchers worldwide [1-2, 3]. Consequently, this fueled the recent developments of standalone microgrids with RES, energy storage, power electronics, and high-performance energy conversion systems. Robust smooth control plays a crucial role in energy conversion systems in microgrid applications. More recently, new technological developments and researches are exploited in order to face the rising scenario in which low to medium-energy power-generators and storage systems are integrated with the grid. The integration of this technology with

microgrids has recently drawn the attention to address the issue of the rising RES penetration into the network [4]. The microgrid strategy provides the final user to produce and store power so that the microgrid can import or export energy to the grid [1]. The DC microgrids, in particular, are gaining an increased attention from researchers worldwide [5-7]. In this perspective, numerous studies are suggested and discussed in the literature of smart grids and power electronics that deal with the control of such systems [8-10].

Influenced by the rapid developments of renewable energy, power electronics, and smart grids, switching DC-DC converters are becoming essential nowadays. For their low cost, high power efficiency and simple structure, their many end-user applications [11] range from fuel and solar cells [12, 13], portable electronic devices [14], DC microgrids and motor drives [15], electric and hybrid vehicles [16, 17], to photovoltaic systems [18] and wind turbine generators [19]. As mentioned in [11], there are two main control application challenges that must be addressed for the converters to match the source and the load; these energy sources are subject to disturbances and variations due to environmental conditions while each of them has different energy generation characteristics that should be properly addressed. Control challenges are inherent from the system internal characteristics [20] including the switched nature, nonlinearities, non-minimum phase behavior and input as well as state constraints.

This paper considers the problem of DC-DC buck converter control while accounting for its unique characteristics in practical implementations. The objective of the designed controller is to ensure different criteria of high robustness, fast response with good dynamic performance, and reliability in practical implementation. The recent developments in this field attracted a great attention to develop smart controllers for DC-DC buck converters. In general, conventional control methodologies are designed through various levels of approximations and simplifications whereas destined for different but individual performance criteria such as source disturbances, load variation, fast transient, overcurrent protection, or tracking error. [21] conducted a comparison of recent optimal and hybrid control methods for DC-DC buck converters which are grouped into five control techniques. Stability analysis and comparison of

conventional controllers are provided in [22] for photovoltaic powered buck- DC-DC converters; [22] where fuzzy logic controllers [23] showed better performance compared to classical PI controllers [24, 25]. Performance comparison of traditional controllers for DC-DC buck converter was conducted in [26]. In this paper, the existing approaches are referred to as linear and nonlinear techniques. We call linear approaches all those which assume linearity characteristics such as a linear model for the DC-DC buck converter system and/or linear effects or utilize linear controllers and/or linear observers. Nonlinear control techniques do not make any linearity assumption and they can be classified into artificial, analytical, and knowledge-based.

As conducted in [27], linear control techniques are advantageous in terms of low complexity and higher reliability in DC-DC buck converter control systems. The classical Proportional-Integral-Derivative (PID) and H_∞ controllers were presented and compared in [28] to reduce the oscillatory behavior in wind power generation applications. However, [29] highlighted the requirement for overcurrent protection and proposed an extension to the classical PID controller called current-constrained PID controller. A linear state-feedback controller was presented in [30] for optimal control of DC–DC buck converters assuming a Markov jump linear system. While a large class of linear control techniques focuses on tracking performance, a second class focuses on robustness issues and disturbance rejection capabilities. [31] highlighted the global robustness problem in output voltage regulation for DC–DC buck converter systems, a linear discrete-time observer was presented to ensure stability and disturbance rejection. [32] conducted a qualitative robustness analysis of DC–DC buck converters and presented a linear observer called disturbance compensation gain as a solution. In an extension to this, a Generalized-Proportional-Integral (GPI) was developed in [33] for disturbance rejection control in DC–DC buck converters. Alternative disturbance rejection approaches include current sharing through finite-time control [34], tail-current control [35], or dual operation modes [36] for interval robustness only.

Bound to their simplicity, linear control techniques fail to address the nature of the considered problem and ignore many of the actual characteristics, which are unique for various DC–DC buck converter systems and depend on the application. Linearity assumptions in the model are vague approximations that reduce its accuracy while restricting the controller design to linear controllers greatly limits its effectiveness; there are few works in the literature addressing these shortcomings through nonlinear control techniques for efficient energy conversion applications. The closest nonlinear extension to the classical PID controller is the nonlinear fractional order synergetic controller [37] which achieved stability and dynamic tracking performance; despite being more general, this controller is still constrained by its P-I-D structure. A sliding mode controller for DC–DC buck converter systems was presented in [38] focusing mainly on dynamic performance compared to the classical PID controller reported in the above literature. Artificial intelligence techniques are frequently used to tackle the control problem in DC–DC buck converters. A fuzzy controller was proposed in [39] with a focus on dynamic and steady state performance. Fuzzy logic controllers are rule-based and require a lot of expertise and data for the selection of membership functions and fuzzy rules. These drawbacks make rule-based controllers tedious for design and implementation in real life. On the other hand, deep learning techniques are recently reported to deal with this problem. A new control approach based on neural networks was presented in [40] for DC-DC conversion devices while the required large amounts of training data were supplied through simulation trials. A combination of neural networks and fuzzy logic was introduced in [41] where neuro-fuzzy controllers and gain tuners were presented. However, the artificial controllers are known for two main drawbacks in practice; the first shortcoming is due to their trustworthiness issues since it is challenging to ensure their performance and prove their stability in non-tested

situations; the second shortcoming is the requirement for huge training data with extensive time and memory computational resources making their implementation unfeasible in real-world industrial applications. The state-of-the-art artificial controllers are complex and uncommon in practice since DC–DC buck converters remain superior for their desired characteristics of simplicity, reliability, and efficiency.

This paper introduces a novel composite robust nonlinear controller based on a nonlinear observer for DC-DC buck converter control for input voltage and current regulation to achieve a good tracking of the optimal desired voltage and therefore a maximum power point in renewable energy applications. The controller considers input voltage of desired trajectories to ensure Maximum Power Point Tracking (MPPT) used in standalone and microgrid applications. A nonlinear observer is also developed to avoid sensor redundancy and hence reduce complexity and increase cost efficiency. Unlike the reported approaches, the novel controller aims at a good balance between dynamic performance, robustness, and practical implementation. For this purpose, the proposed composite controller design introduces an extra augmented state and the controller parameters are tuned using Particle Swarm Optimization (PSO) algorithm to achieve these criteria in a unique design. PSO is selected in this work due to its simple concept, robustness, and easy implementation, it is known by its capability to avoid local minima. The dynamic performance considers fast transient response, reduced overshoot and minimum oscillation behavior; whereas the robustness considers active source and load disturbance rejection. This work is first verified though extensive simulations and comparisons then validated in experimental applications through multiple scenarios to ensure the stated balance.

The remaining sections of this paper are organized as follows; Section 2 presents a complete model for the DC–DC Buck converter system, followed by the proposed controller design, and the nonlinear state observer. Section 3 then presents simulation and experimental results with comparisons and discussion. The last section summarizes the key aspects of this paper and presents some conclusions.

2. Problem Formulation and Novel Designs

This section presents the design of a new robust low-cost nonlinear controller based on a nonlinear state observer. In addition to the input voltage measurement, we assume only single input current measurement for the DC-DC buck converter (the input current measurement is also needed for many MPPT algorithm techniques), the input voltage V_c should track efficiently a desired trajectory V_{ref} in a finite time. The controller also considers the issues of disturbances, abrupt changes in the reference voltage, input current change, and abrupt variations in the DC voltage.

The proposed control scheme in this study can be used for different power applications such as wind energy systems [42], photovoltaic (PV) energy systems [43], and hydrogen fuel cells [44] as depicted in Fig.1. The overall DC-DC proposed control scheme is explained in details in subsections 2.2 and 2.3.

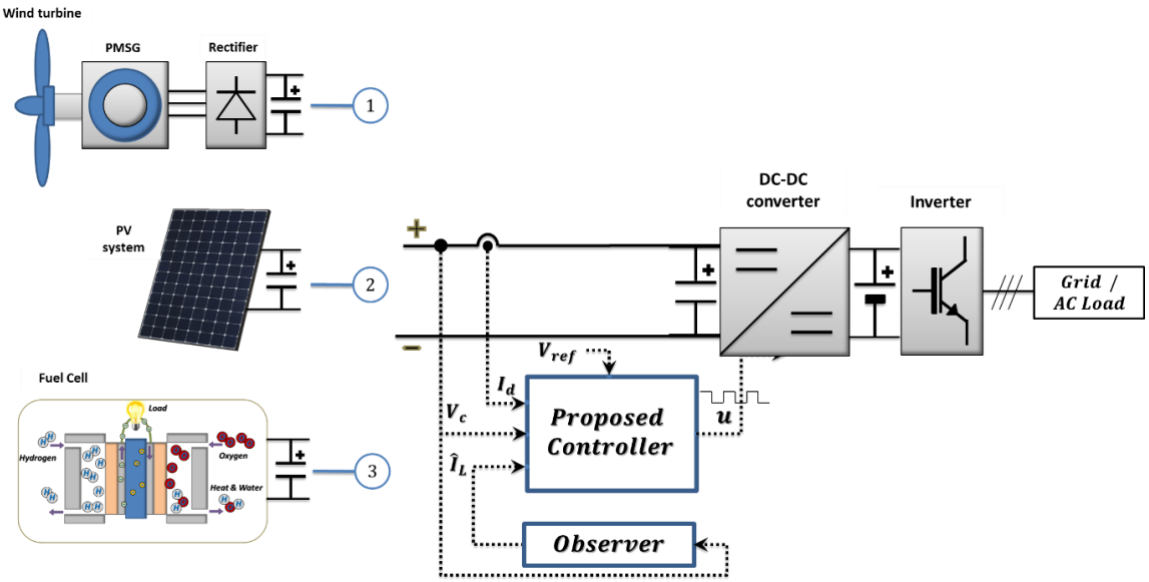

Fig. 1. Overview of the proposed control scheme.

2.1. DC-DC Buck Converter Modelling

Fig. 1 shows a diagram of the proposed scheme of a DC–DC step-down (buck) converter where V_{dc} is the DC link voltage, I_d is the input current and V_c is the input voltage regulated around a constant reference value V_{ref}. This architecture is mostly used in standalone renewable energy applications, where the input voltage should track a desired reference to ensure the MPPT mode.

The instantaneous switched model of the DC-DC buck converter is described as

$$\begin{cases} \frac{dV_c}{dt} = \frac{1}{C}(I_d - \alpha I_L) \\ \frac{dI_L}{dt} = \frac{1}{L}(\alpha V_c - V_{dc} - r_L I_L) \end{cases}, \quad (1)$$

where L is the inductance, r_L is the inductor resistance, and C is the capacitance as shown in Fig. 2, $\alpha \in \{0,1\}$ is the switching control signal that takes only binary values 0 (switch open) and 1 (switch closed).

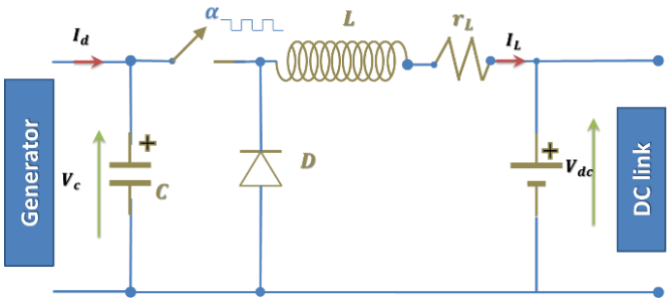

Fig. 2. Schematic diagram of the DC-DC buck converter**.**

The binary signal (α) is the switching command, it is controlled by means of a fixed-frequency Pulse Width Modulation (PWM). The constant switching frequency is $1/T_s$ where T_s is the switching period equal to the sum of T_{on} (when $\alpha = 1$) and T_{off} (when $\alpha = 0$) such that the ratio T_{on}/T_s is the duty-cycle u. Generally, the switching model is represented by the average PWM model [44]:

$$\begin{cases} \frac{dV_c}{dt} = \frac{1}{C}(I_d - \alpha I_L) \\ \frac{dI_L}{dt} = \frac{1}{L}(uV_c - V_{dc} - r_L I_L) \end{cases}, \tag{2}$$

The system state space vector x includes the measured inductor current I_L and the input voltage V_c

$$x = [I_L \quad V_c]^T, \tag{3}$$

In order to ensure zero steady-state error in the output voltage V_c from its reference value V_{ref}, Eq. (2) is then augmented with another additional state variable x_1 which stands for the integral of the output voltage V_c, the augmented nonlinear state-space model is then given by

$$\begin{cases} \frac{dx_1}{dt} = V_c \\ \frac{dV_c}{dt} = \frac{1}{C}(I_d - \alpha I_L) \\ \frac{dI_L}{dt} = \frac{1}{L}(uV_c - V_{dc} - r_L I_L) \end{cases}, \tag{4}$$

2.2. The Proposed Controller Design

The proposed controller design in this work introduces a three-states error vector that represents the instantaneous as well as the cumulative errors to assess both transient and robustness criteria. The design also incorporates a sliding mode control strategy which includes two main steps. A sliding surface is first selected to force the system states to a predefined surface. A discontinuous state feedback control law is then designed to force the controlled system to attain the states on the surface in a finite time.

The error vector comprises the integral of the output voltage tracking error (e_1), the voltage tracking error (e_2), and also the current tracking error (e_3) which are defined as

$$\begin{cases} e_1 = \int (V_{ref} - V_c) dt \\ e_2 = V_{ref} - V_c \\ e_3 = I_{L_{ref}} - I_L \end{cases}, \tag{5}$$

where $I_{L_{ref}}$ represents the reference current generated by the voltage loop controller, and V_{ref} represents the desired output voltage of the buck converter.

According to Eq. (5), the time derivatives of the errors e_i are derived as

$$\begin{cases} \dot{e}_1 = e_2 \\ \dot{e}_2 = -\dot{V}_c \\ \dot{e}_3 = \dot{I}_{L_{ref}} - \dot{I}_L \end{cases} \tag{6}$$

In order to ensure the stability of the system, the reference current $I_{L_{ref}}$ is proposed as

$$I_{L_{ref}} = \frac{C}{u}\left(\frac{I_d}{C} - (1 + \lambda_1\lambda_2)e_1 - (\lambda_1 + \lambda_2)e_2\right), \tag{7}$$

where λ_1 and λ_2 are real positive numbers.

Remark 1. The number of sliding surfaces depends on the number of state variables. In this case, there are three states for the augmented model of the buck converter as given in Eq. (4), so three sliding surfaces are defined in this context.

The proposed sliding surface $S(t)$ is designed as

$$S(e,t) = [S_1 \quad S_2 \quad S_3]^T, \tag{8}$$

where

$$\begin{cases} S_1 = e_1 \\ S_2 = e_2 + \lambda_1 e_1, \\ S_3 = \sqrt{L/C}\, e_3 \end{cases} \tag{9}$$

The control input must therefore ensure the following condition:

$$S\dot{S}^T < 0 \tag{10}$$

Manipulating Eqs. (4)-(10) yields

$$\begin{aligned} S\dot{S}^T = e_1 e_2 + (e_2 + \lambda_1 e_1)\left(-\frac{1}{C}(I_d - uI_L) + \lambda_1 e_2\right) \\ + e_3\left(\dot{I}_{L_{ref}} - \frac{1}{L}(uV_c - V_{dc} - r_L I_L)\right), \end{aligned} \tag{11}$$

which can be rewritten as

$$\begin{aligned} S\dot{S}^T = e_1(e_2 + \lambda_1 e_1 - \lambda_1 e_1) + (e_2 + \lambda_1 e_1)\left(-\frac{1}{C}(I_d - uI_L) + \lambda_1 e_2\right) \\ + \frac{L}{C} e_3\left(\dot{I}_{L_{ref}} - \frac{1}{L}(uV_c - V_{dc} - r_L I_L)\right), \end{aligned} \tag{12}$$

and simplified into

$$S\dot{S}^T = -\lambda_1 e_1^2 + (e_2 + \lambda_1 e_1)\left(e_1 + \frac{u}{C} I_{L_{ref}} - \frac{1}{C}(I_d + u e_3) + \lambda_1 e_2\right) + \frac{L}{C} e_3 \left(\dot{I}_{L_{ref}} - \frac{1}{L}(u V_c - V_{dc} - r_L I_L)\right), \quad (13)$$

Replacing $I_{L_{ref}}$ in Eq. (13) by its expression in Eq. (7) results in

$$S\dot{S}^T = -\lambda_1 e_1^2 - \lambda_2 (e_2 + \lambda_1 e_1)^2 + e_3 \left(\frac{L}{C}\dot{I}_{L_{ref}} - \frac{1}{C}(u V_c - V_{dc} - r_L I_L) - \frac{u}{C}(e_2 + \lambda_1 e_1)\right). \quad (14)$$

In order to ensure the condition Eq. (10); based on Eq. (14), the resulting control law (u) is derived as

$$u = \frac{C}{(V_{ref} + \lambda_1 e_1)}\left(\frac{1}{C}(V_{dc} + r_L I_L) + \frac{L}{C}\dot{I}_{L_{ref}} + \lambda_3 e_3 + \lambda_4 sign(e_3)\right). \quad (15)$$

This ensures the condition

$$S\dot{S}^T = -\lambda_1 e_1^2 - \lambda_2 (e_2 + \lambda_1 e_1)^2 - \lambda_3 e_3^2 - \lambda_4 |e_3| < 0. \quad (16)$$

Thus, the derivative of the Lyapunov function Eq. (16) is definite negative, which confirms the stability and the convergence of the proposed nonlinear control strategy.

Remark 2. Besides ensuring stability and convergence of the controlled system, better tracking performance is ensured by selecting ideal gains of each controller. Therefore, parameters of the proposed controller ($\lambda_1, \lambda_2, , \lambda_3$ and λ_4), and the parameters of the conventional PI controller (for comparison) (K_p and K_i) are tuned using the metaheuristic Particle Swarm Optimization (PSO) algorithm[45-47] to minimize the IAE (Integral Absolute-value of the Error) fitness function, as explained by the proposed block diagram shown in Fig. 3. (Refer to details in[47-49]).

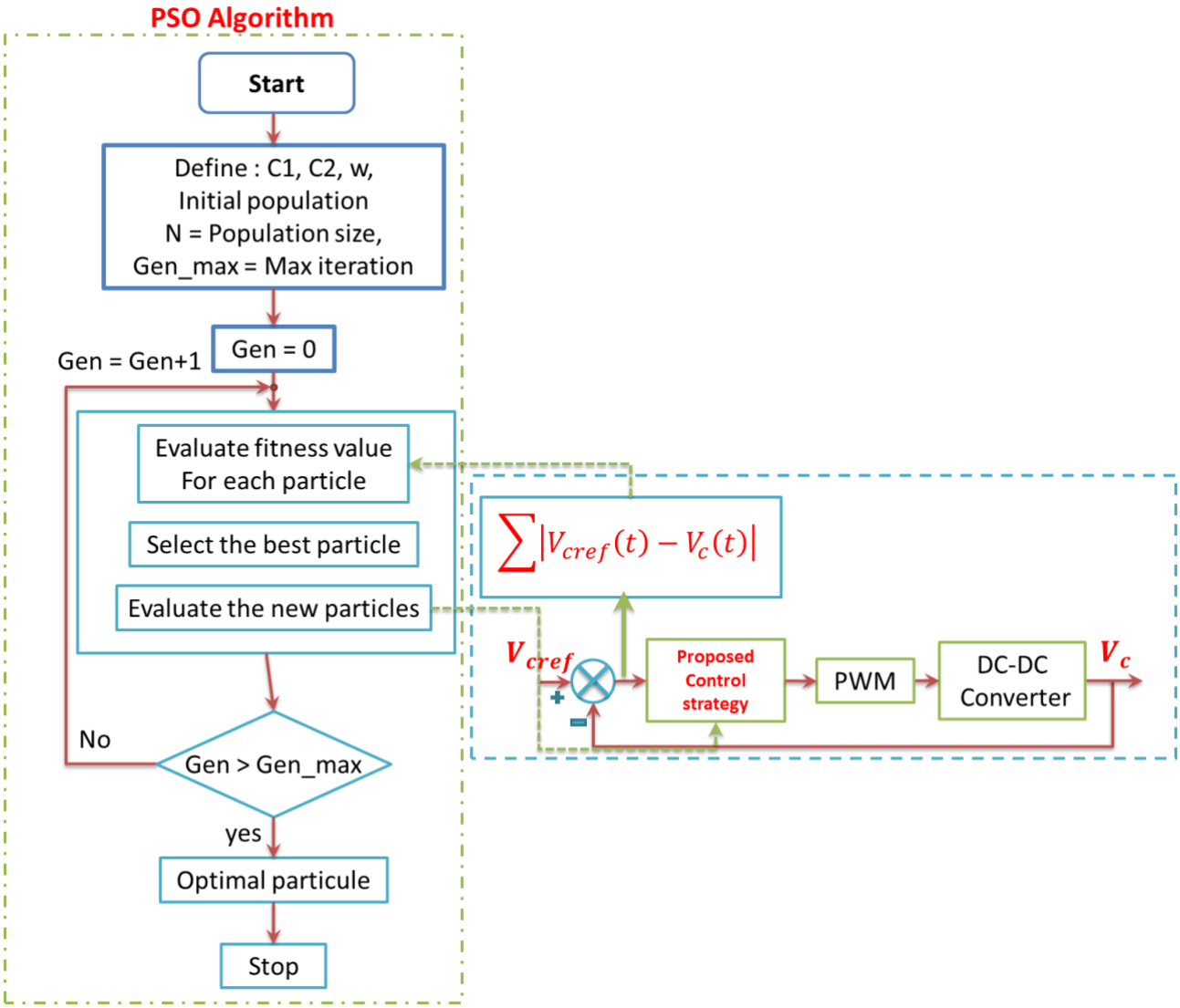

Fig. 3. Proposed block diagram of PSO-based controller design.

2.3. The Proposed Nonlinear State Observer

In order to assure the new nonlinear controller design is robust and cost-efficient in practical implementations, a nonlinear state observer is also designed. This allows to avoid sensor redundancy and ensure cost-efficiency by avoiding the additional sensor for the output current. In this work, the inductor current I_L is estimated by means of the proposed nonlinear state observer which will be used as part of the controller design.

The proposed observer has the following structure which may also be used for fault tolerant control purposes:

$$\begin{cases} \frac{d\hat{V}_c}{dt} = \frac{1}{C}\left(I_d - u\hat{I}_L + k_1\tilde{z}_1\right) \\ \frac{d\hat{I}_L}{dt} = \frac{1}{L}\left(-V_{dc} - r_L\hat{I}_L + u\hat{V}_c + k_2 u\,\tilde{z}_2\right) \end{cases}, \tag{17}$$

where

$$\begin{cases} \tilde{z}_1 = \hat{V}_c - V_c \\ \tilde{z}_2 = \hat{I}_L - I_L \end{cases}. \tag{18}$$

Then, the error dynamics of Eq. (17) and Eq. (18) are obtained as

$$\begin{cases} \dot{\tilde{z}}_1 = \frac{1}{C}(-u\tilde{z}_2 + k_1\tilde{z}_1) \\ \dot{\tilde{z}}_2 = \frac{1}{L}(u\tilde{z}_1 - r_L\tilde{z}_2 + k_2 u\tilde{z}_1) \end{cases}, \tag{19}$$

choosing $k_2 = -1$, then Eq. (19) will reduce to

$$\begin{cases} \dot{\tilde{z}}_1 = \frac{1}{C}(-u\tilde{z}_2 + k_1\tilde{z}_1) \\ \dot{\tilde{z}}_2 = -\frac{r_L}{L}\tilde{z}_2 \end{cases}, \tag{20}$$

This is solved by defining the following Lyapunov candidate function

$$V_3 = \frac{L}{2}\hat{z}_2^2 + \frac{C}{2}(\hat{z}_1 - \psi\,\hat{z}_2)^2, \tag{21}$$

with $\psi = \frac{u}{r_L C/L + k_1}$. The time derivative of the proposed Lyapunov function Eq. (21) is:

$$\dot{V}_3 = -r_L\hat{z}_2^2 + k_1(\hat{z}_1 + \psi\,\hat{z}_2)(\hat{z}_1 - \psi\hat{z}_2). \tag{22}$$

The derivative of Lyapunov function V_3, as in Eq. (22), is negative definite if the condition is satisfied $k_1 < 0$, which guarantees the convergence of the proposed observer where the unknown value of k_1 can be tuned using the same PSO algorithm as mentioned in Remark 1.

3. Simulation and Experimental Validation

In order to demonstrate the feasibility and the effectiveness of the closed-loop system under the proposed control strategy, simulation and experimental results are given in this section. Furthermore, in order to verify the control performance of the proposed control law, the common Proportional-Integral (PI) controller is used for comparison. Controller gains were optimally tuned using the PSO algorithm. The corresponding PI controller has the following structure:

$$u = 1 - \left(K_p(V_{ref} - V_c) + K_i \int (V_{ref} - V_c)\ dt \right) \tag{23}$$

Fig. 4 represents the schematic diagram of the connection for software and hardware configurations of the proposed control study.

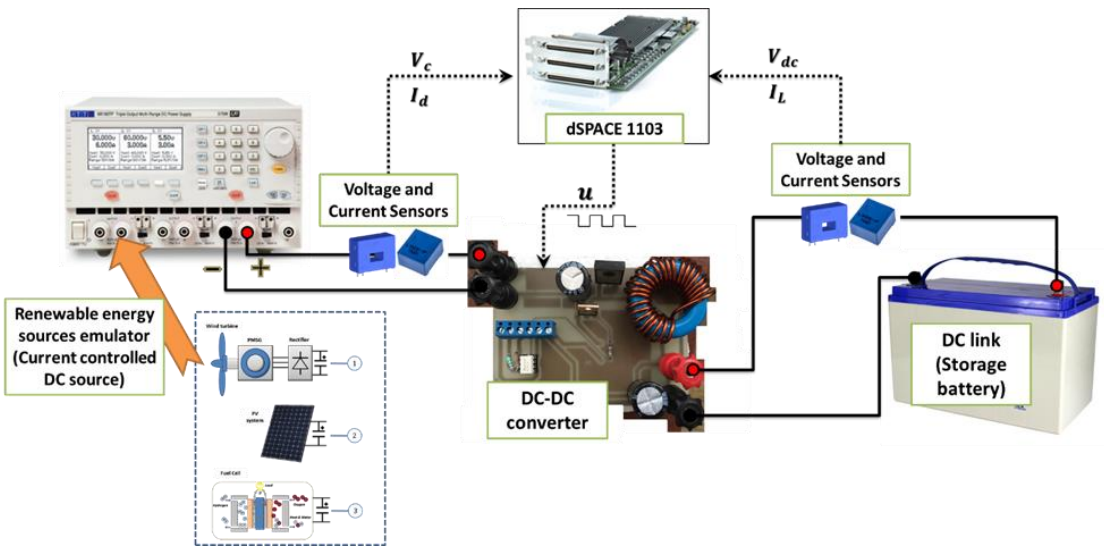

Fig. 4. Block diagram showing connections for software and hardware configurations of the proposed control study.

3.1. Simulation Results and Analysis

To demonstrate the effectiveness and to comprehensively evaluate the performance of the proposed control scheme, a tuned PI controller was selected as a reference for comparison since PI controllers are the widely common designs for this problem. In this paper, three different validation scenarios are provided in a simulation study to test (i) the observer's robustness for state estimation under disturbances, (ii) steady-state and transient performance during reference voltage changes, and (iii) robustness against sudden input current change with abrupt variations in DC voltage. Table 1 lists the main parameters of the DC-DC buck converter that is used in this application.

Table 1. Main parameters of the DC-DC buck converter.

Parameters	Value
R_L	0.2Ω
V_{dc}	$400V \mp 10V$
C	$500\mu F$
L	$200\mu H$
I_d	$10\ A$
V_{dc}	$96\ V$

A Matlab/Simulink model was developed to simulate the proposed control strategies as shown in Fig. 5.

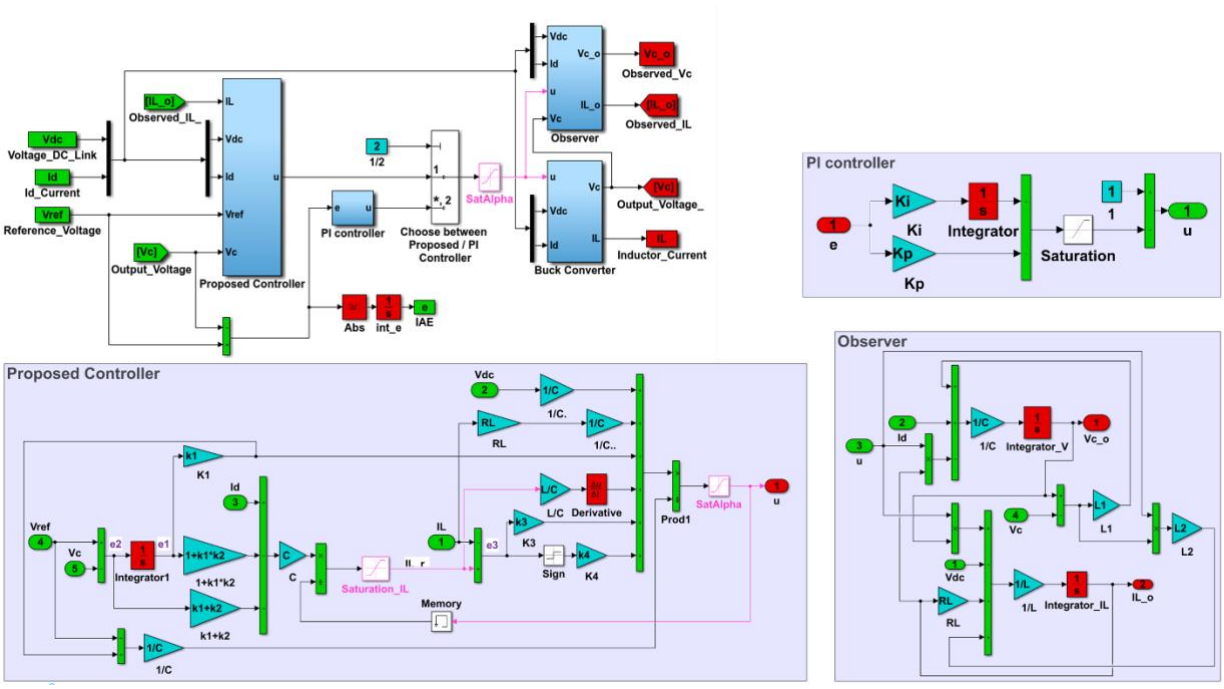

Fig. 5. Simulation model of the controlled system with the proposed controllers in Matlab/Simulink.

The tuned parameters of the reference PI and the proposed controllers as well as the proposed observers are listed in Table 2.

Table 2. Controllers' and observer's parameters

Controller	Notations	Gains
Tuned-PI controller	k_P	0.5
	k_i	0.02
Proposed controller	λ_1	20
	λ_2	01
	λ_3	100
	λ_4	08
Proposed Observer	k_1	-1000
	k_2	-1

- **Scenario one** test the effects of disturbances on the designed observer: in this scenario, the proposed observer's estimated states are compared to real states starting from different initial conditions; Besides, voltage and current disturbances (ΔV and ΔI) are injected at t = 0.05s. It can be deduced from Fig. 6 that the estimated state variables match their real values regardless of the large disturbance size. This confirms the

effectiveness of the proposed observer for fast, accurate, and robust states estimation. Furthermore, comparisons of the rise time (the time required to reach 90% of the desired value [1]), the output voltage and current errors are given in Table 3. With negligible rise time values, Table 3 and Fig. 6 demonstrate the accurate estimation of the system states using the proposed observer with a short rise time and less error values even during disturbances.

Table 3: Comparison of rise time, output voltage and current error values for the designed observer for test Scenario 1 (simulation case).

Rise time	0.0025s	**Rise time**	0.0012 sec
Introduced $\boldsymbol{\Delta V}$	15 %	Introduced $\boldsymbol{\Delta I}$	65 %

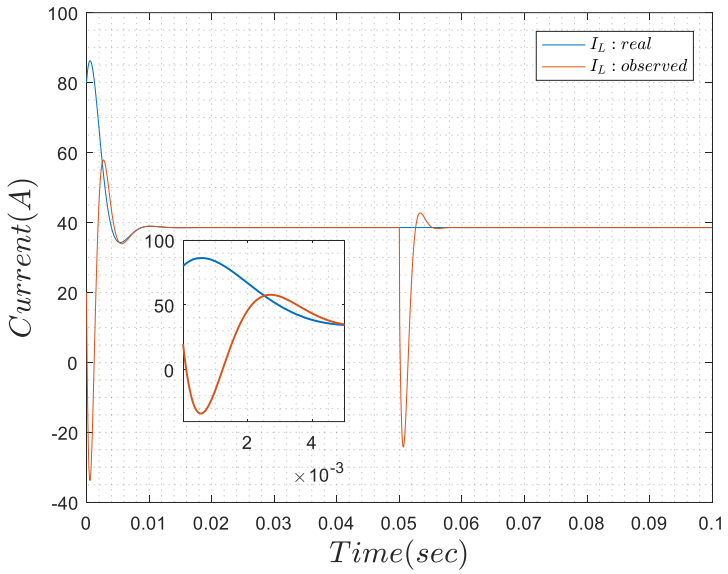

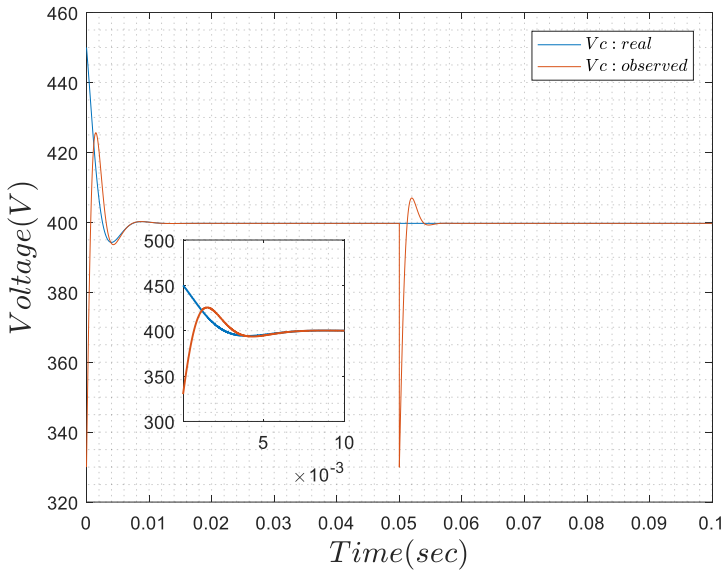

Fig. 6. Real versus estimated states (a) inductor current; (b) output voltage in Scenario 1.

- **Scenario two** tests the dynamical performance in the case of reference voltage changes: in this scenario, the reference voltage of the DC-DC buck converter changed as follows:

$$V_{ref} = \begin{cases} 380\text{V} & 0.0 \leq \text{t} \leq 0.1 \text{ sec} \\ 420\text{V} & 0.1 \leq \text{t} \leq 0.2 \text{ sec} \\ 400\text{V} & 0.2 \leq \text{t} \leq 0.3 \text{ sec} \\ 360\text{V} & 0.3 \leq \text{t} \leq 0.4 \text{ sec} \end{cases} \quad (24)$$

The reference trajectory tracking (for inductor current and output voltage) performance of the proposed controller and the tuned PI controller are presented in Fig. 7. The results show that the proposed nonlinear controller yields superior performance in terms of the reduced settling time, faster convergence of the system response, and the damping of overshoots as compared to a tuned PI controller. It can be concluded that the proposed controller ensures optimum and satisfactory tracking response for a given reference trajectory.

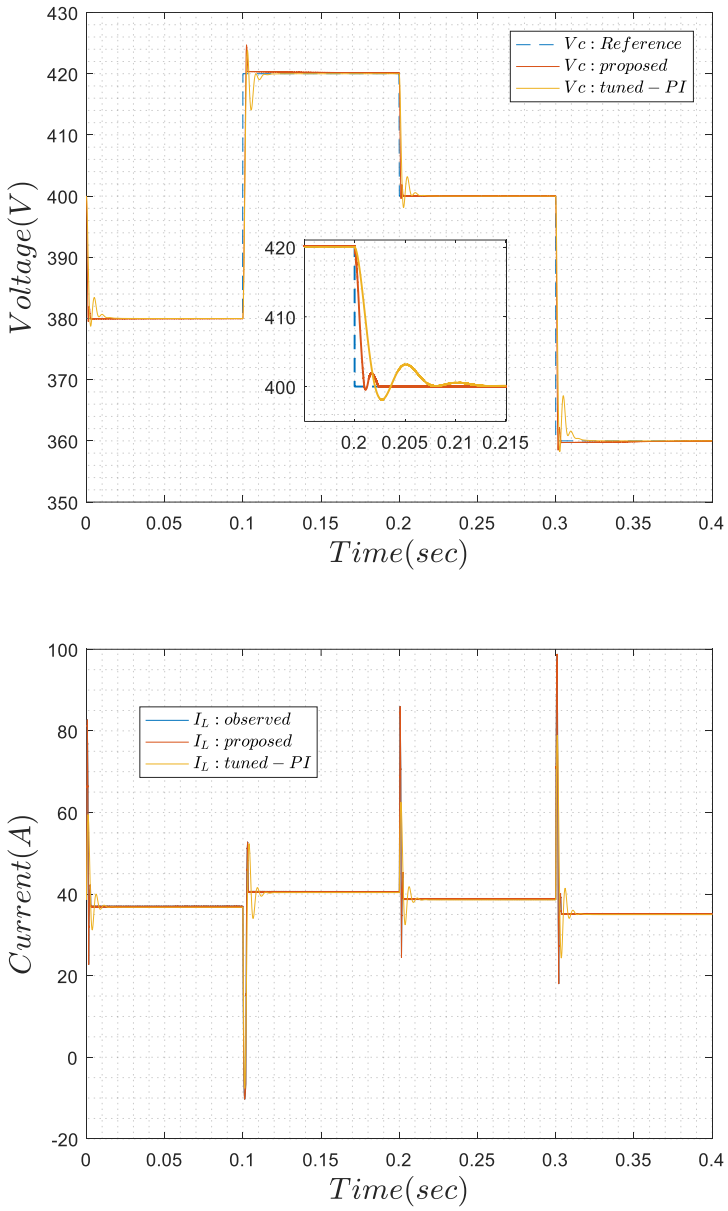

Fig. 7. Comparison of tracking performance under varying reference values (a) output Voltage; (b) inductor current in scenario 2.

- **Scenario three** tests the robustness against sudden input current change with abrupt variations in DC voltage. The input current changes with abrupt variations in DC voltage in this test, an abrupt change of +40% in input current I_d is introduced at t=0.05s and -18% in DC voltage V_{dc} at t=0.15s. The corresponding output voltage and inductance current responses are shown in Fig. 8. It can be observed that the proposed controller has better disturbance rejection and higher effectiveness in tracking reference values

during abrupt variations in the inductor current and DC voltage compared to the tuned PI controller which exhibits a longer oscillation ~~duration~~ before reaching a steady sate.

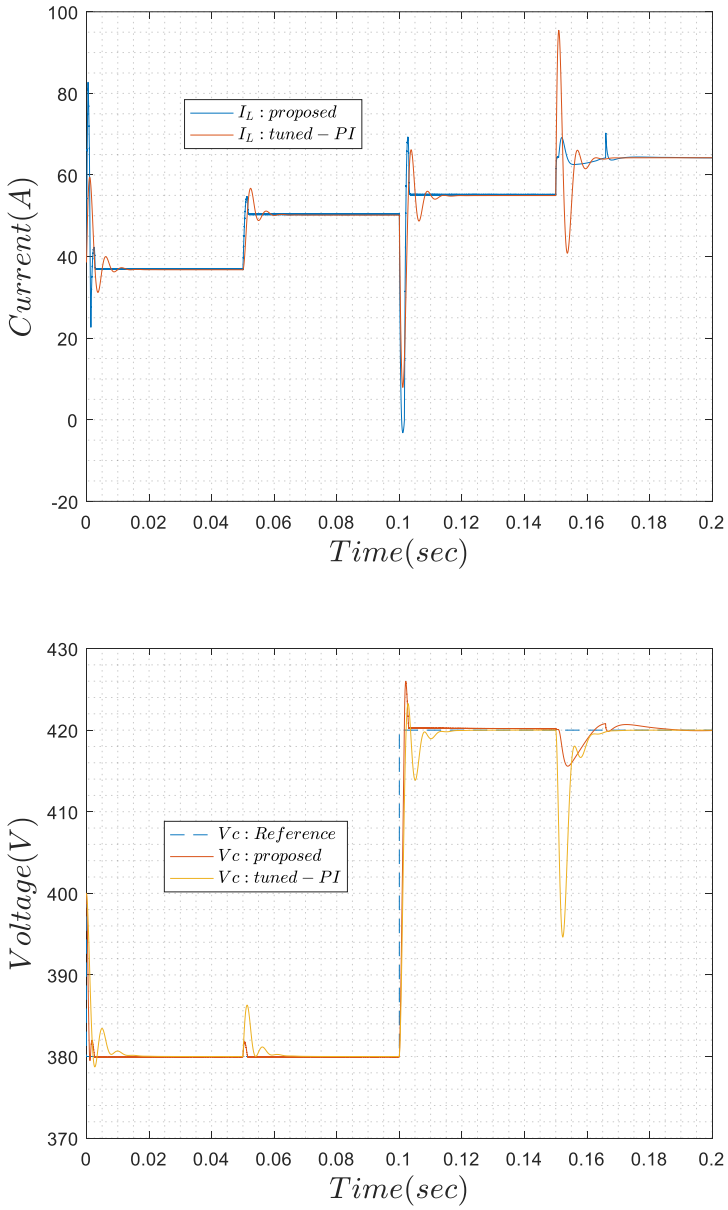

Fig. 8. Comparison of tracking performance under abrupt variations in DC voltage and Input current for: (a) output voltage; (b) current inductor in scenario 3.

The observations of rise time, overshoot, and performance index (IAE) are listed in Table 4. Table 4 demonstrates that the proposed controller has a smaller overshoot, a short rise time and a reduced IAE value as compared to the tuned PI controller. The

ability of the proposed control scheme to reject disturbances [50-52] and tolerate faults [20, 26, 39] can be further investigated in future works.

Table 4. Comparison of Rise time, Overshoot and IAE performance index between the proposed controller and a tuned PI controller (lower is better).

	T=0.05sec (Overshoot)	**T=0.10 sec (Rise time)**	**T=0.15 sec (Overshoot)**	**IAE (performance index)**
Proposed controller	0.47 %	0.015	1.29 %	0.106
Tuned PI controller	1.66 %	0.019	6.04 %	0.210

3.2. Experimental Results

Experimental applications are also conducted in this work to verify the advantages of the proposed control strategy compared to a tuned PI controller. Different tests for the DC-DC buck converter are performed experimentally as shown in Fig. 9. The experimental setup consists of a DC source emulator that generates a controlled DC current, a 12V battery (DC link) and a DC-DC buck converter. The proposed control strategy is implemented in real time using a dSPACE 1103 control board which also allows data acquisition and storage from the different sensors. The parameters of the DC-DC buck converter were selected similar to those in the simulation study above, two scenarios were evaluated and their parameter settings are similar to those in the simulation.

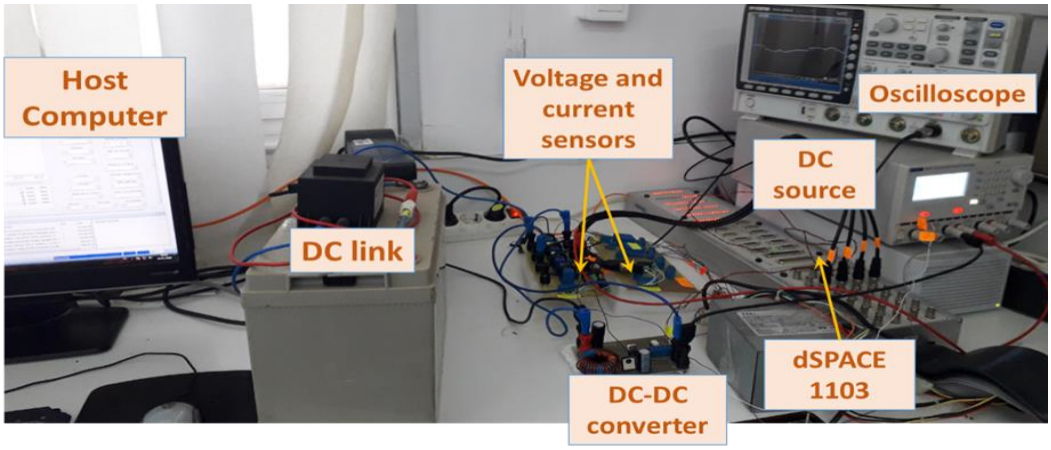

Fig. 9. Experimental test setup.

- **Scenario one**: in this test, the proposed observer's estimated states are compared to real states starting from different initial conditions. In addition, disturbances (ΔV and ΔI) are injected at t = 1.88s. Measured and estimated states of this scenario are illustrated in Fig. 10; the estimated state variables remain close to their real values, this confirms the effectiveness of the proposed observer for real-time state estimation. Table 5 lists the rise time observations which have negligible values reflecting a very short duration for the observer to reach steady-state after the disturbance.

Table 5. Comparison of rise time, output voltage and current error values for the designed observer (experimental case).

Rise time	0.0310sec	**Rise time**	0.0460sec
$\boldsymbol{\Delta V}$	110 %	$\boldsymbol{\Delta I}$	440 %

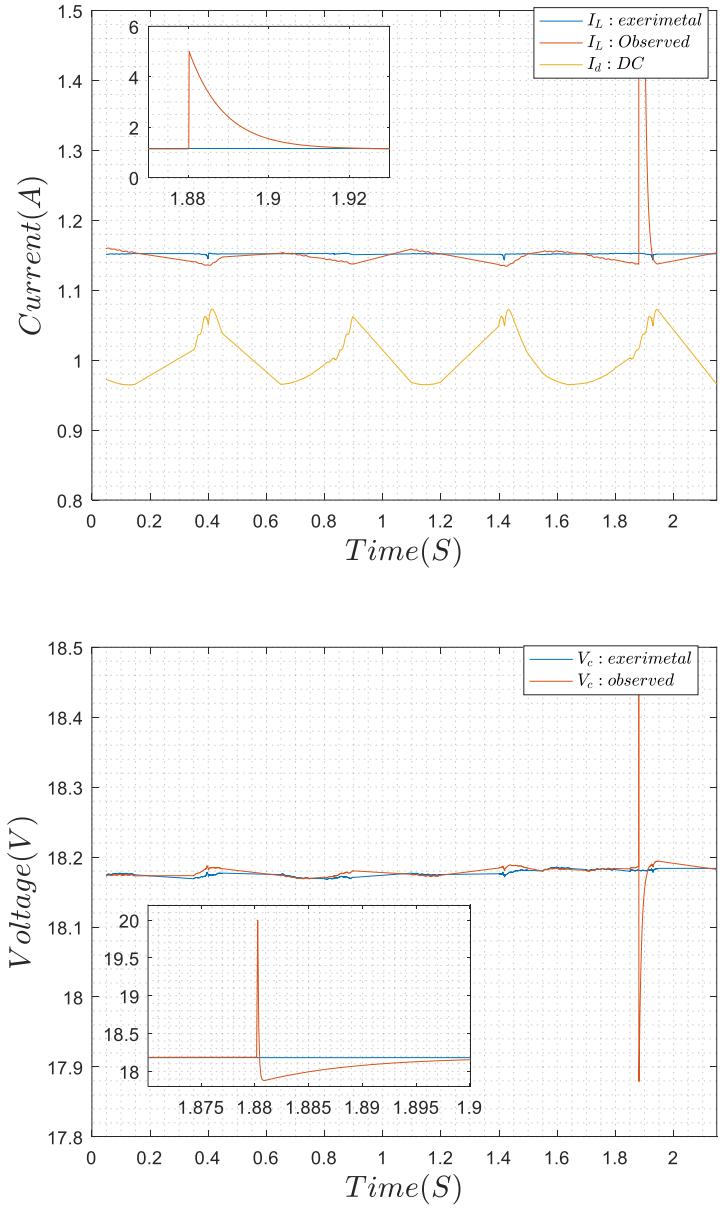

Fig. 10. Real and observed states: (a) inductor current; (b) output voltage in experimental Scenario 1**.**

- **Scenario two**: in this test, the controller follows a given reference voltage. The patterns of voltage tracking reference, the inductor current, and the output voltage are presented in Fig. 11 and Fig. 12 showing respectively the responses of the proposed control strategy and a tuned PI controller. The results show that the proposed controller yields superior performance in terms of a reduced rise time for faster convergence of the system responses as compared to a tuned PI controller; these results are also listed

in Table 6. It can be concluded that the proposed controller ensures superior and satisfactory tracking response for a given reference trajectory.

Table 6. Comparison of rise time between the proposed and a tuned PI controller for experimental Scenario 2 (lower is better).

Proposed control strategy	**Time**	T= 3.3sec	T=4.5sec	T=8.5sec	T=10.8sec
	Rise time	**0.040**	**0.017**	**0.017**	**0.016**
Tuned PI controller	**Time**	T=2.6 s	T=6.5 s	T=8.4 s	T=12.7s
	Rise time	0.261	0.195	0.230	0.287

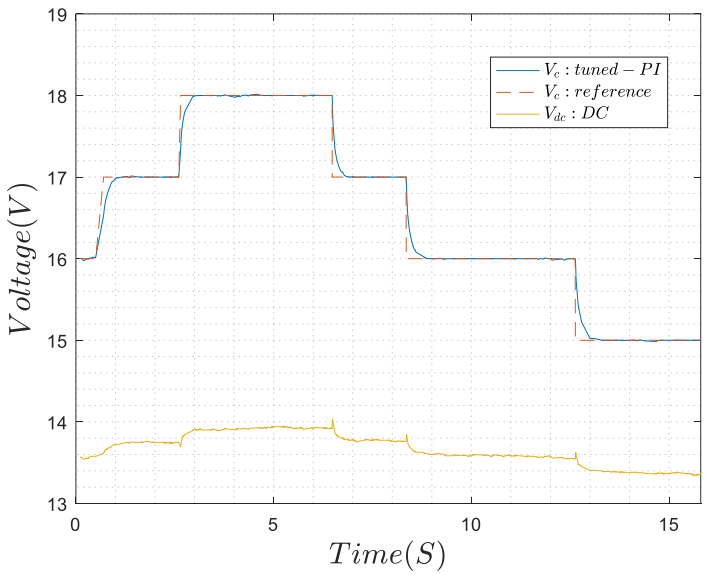

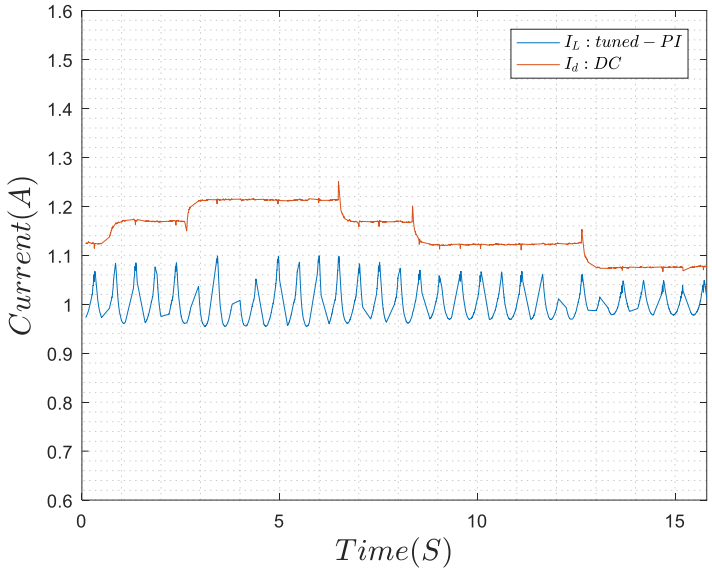

Fig. 11. Tracking performance of the classical PI controlled system under varying reference values (a) output voltage; (b) inductor current in experimental Scenario 2.

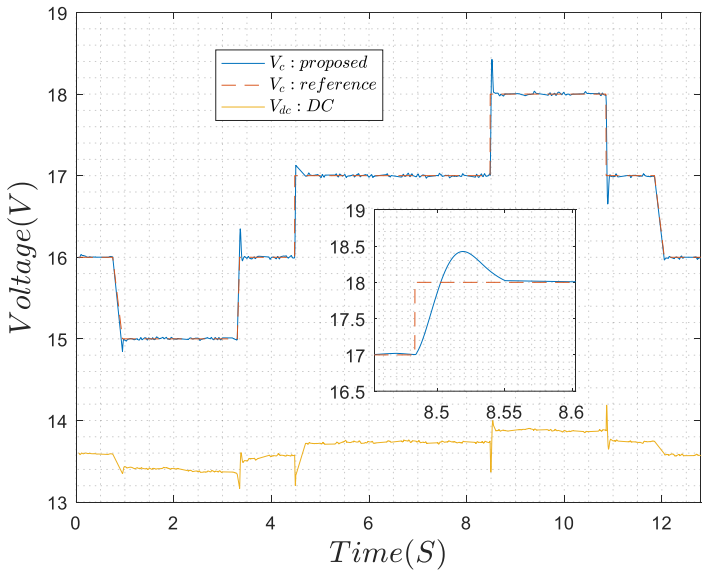

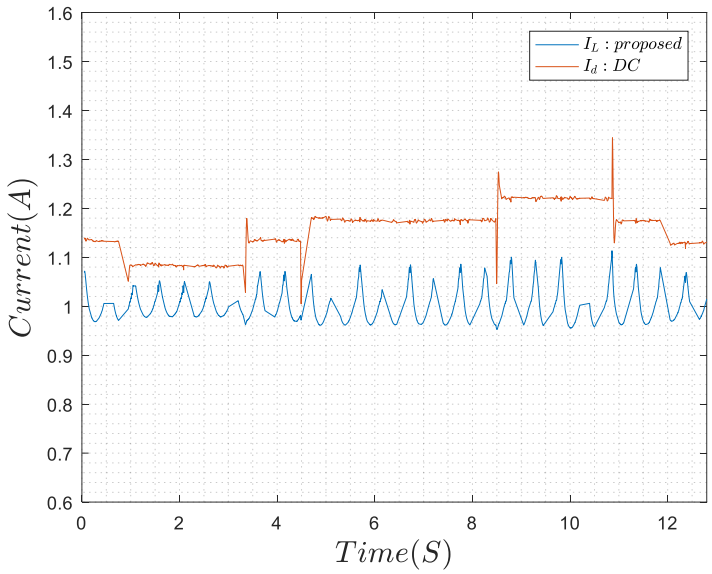

Fig. 12. Tracking performance of the proposed controlled system under varying reference values (a) output voltage; (b) inductor current in experimental Scenario 2.

4. Conclusions and Perspectives

This work introduced a composite robust nonlinear control scheme through a nonlinear state observer for DC-DC buck converter control to achieve a good voltage tracking in renewable energy applications. The controller was designed with three main advantages making a good balance between dynamic tracking performance, robustness to source and load variations, and practical implementation. The stability conditions of the closed-loop system are demonstrated based on Lyapunov theory. The conducted analysis included different test scenarios on state estimation, trajectory tracking, and active disturbance rejection. The simulation and experimental implementation results showed the superior effectiveness of the proposed controller in terms of improved tracking dynamics of the output voltage trajectory, offering shorter rise time compared to a tuned PI controller. Furthermore, the proposed controller exhibits the remarkable ability of rejecting external disturbances in DC voltage and input current. The design was proved advantageous for its flexibility for realization in real energy

conversion applications and its cost-efficiency. Future works may consider an extension of the proposed controller capabilities to intelligent fault detection and fault-tolerant control.

References

[1] A. Dali, S. Diaf, M. Tadjine, Maximum Power Tracking and Current Control for Solar Photovoltaic System Applications, Hybrid Dynamical System Approach, Journal of Dynamic Systems Measurement and Control, 141(9) (2019) 091017-091025.

[2] A. Haque, Maximum Power Point Tracking (MPPT) Scheme for Solar Photovoltaic System, Energy Technology & Policy, 1(1) (2014) 115-122.

[3] N. Vafamand, M. Rakhshan, Dynamic Model-Based Fuzzy Controller for Maximum Power Point Tracking of Photovoltaic Systems: A Linear Matrix Inequality Approach, Journal of Dynamic Systems Measurement and Control, 139(5) (2017) 051010-051016.

[4] J. M. Guerrero, J. C. Vasquez, J. Matas, M. Castilla, L. G. d. Vicuna, Control Strategy for Flexible Microgrid Based on Parallel Line-Interactive UPS Systems, IEEE Transactions on Industrial Electronics, 56 (2009) 726-736.

[5] S. Singh, A. R. Gautam, D. Fulwani, Constant power loads and their effects in DC distributed power systems: A review, Renewable and Sustainable Energy Reviews, 72 (2017) 407-421.

[6] E. Planas, J. Andreu, J. I. Gárate, I. Martínez de Alegría, E. Ibarra, AC and DC technology in microgrids: A review, Renewable and Sustainable Energy Reviews, 43 (2015), 726-749.

[7] A. A. Mohamed, A. T. Elsayed, T. A. Youssef, O. A. Mohammed, Hierarchical control for DC microgrid clusters with high penetration of distributed energy resources, Electric Power Systems Research, 148 (2017) 210-219.

[8] M. Hejri, A. Giua, Hybrid modeling and control of switching DC-DC converters via MLD systems, IEEE Conference on in Automation Science and Engineering (CASE), (2011), 714-719.

[9] H. Abouobaida, M. Cherkaoui, M. Ouassaid, Robust maximum power point tracking for photovoltaic cells: A backstepping mode control approach, International Conference on in Multimedia Computing and Systems (ICMCS), (2011) 1-4.

[10] A. Dali, S. Diaf, M. Tadjine, Observer-based control of a photovoltaic DC–DC buck converter: HDS approach, Asian Journal of Control, 21(4) (2019) 1927-1940.

[11] A. Mirzaei, A. Jusoh, Z. Salam, Design and implementation of high efficiency non-isolated bidirectional zero voltage transition pulse width modulated DC–DC converters, Energy, 47(1) (2012) 358-369.

[12] H. Wang, A. Gaillard, D. Hissel, A review of DC/DC converter-based electrochemical impedance spectroscopy for fuel cell electric vehicles, Renewable energy, 141 (2019) 124-138.

[13] F. Dadouche, O. Bethoux, J. P Kleider, New silicon thin-film technology associated with original DC–DC converter: An economic alternative way to improve photovoltaic systems efficiencies, Energy, 36(3) (2011) 1749-1757.

[14] Y. C. Hsu, C. Y. Ting, L. S Hsu, J. Y Lin, C.C.P Chen, A Transient Enhancement DC–DC Buck Converter With Dual Operating Modes Control Technique, IEEE Transactions on Circuits and Systems II: Express Briefs, 66(8) (2018) 1376-1380.

[15] Z. Wang, S. Li, Q. Li, Discrete-Time Fast Terminal Sliding Mode Control Design for DC-DC Buck Converters with Mismatched Disturbances, IEEE Transactions on Industrial Informatics, 16(2) (2019) 1204 – 1213.

[16] S. Pirouzi, J. Aghaei, T. Niknam, M. Shafie-Khah, J.P. Vahidinasab, Two alternative robust optimization models for flexible power management of electric vehicles in distribution networks, Energy, 141 (2017) 635-651.

[17] B. Yang, T. Zhu, X. Zhang, J. Wang, H. Shu, S. Li, T. Yu, T, Design and implementation of Battery/SMES hybrid energy storage systems used in electric vehicles: A nonlinear robust fractional-order control approach, Energy, 191 (2020) 116510.

[18] S. Daraban, D. Petreus, C. Morel, A novel MPPT (maximum power point tracking) algorithm based on a modified genetic algorithm specialized on tracking the global maximum power point in photovoltaic systems affected by partial shading, Energy, 74 (2014) 374-388.
[19] R. Melício, V. M. F Mendes, J. P. D. S. Catalão, Comparative study of power converter topologies and control strategies for the harmonic performance of variable-speed wind turbine generator systems, Energy, 36(1) (2011) 520-529.
[20] S. Abdelmalek, A. T. Azar, D. Dib, A novel actuator fault- tolerant control strategy of dfig-based wind turbines using Takagi-Sugeno multiple models, International Journal of Control Automation and Systems, 16 (2018) 1415–1424.
[21] S. Mariéthoz, S. Almér, M. Bâja, A.G. Beccuti, D. Patino, A. Wernrud, U.T. Jonsson, Comparison of hybrid control techniques for buck and boost DC-DC converters. IEEE transactions on control systems technology, 18(5) (2009) 1126-1145.
[22]. M. E. Şahin and H.İ. Okumuş, *Comparison of Different Controllers and Stability Analysis for Photovoltaic Powered Buck-Boost DC-DC Converter.* Electric Power Components and Systems, 46(2018) 149-161.
[23] M. E. Sahin, and H. I. Okumus, Fuzzy logic controlled parallel connected synchronous buck DC-DC converter for water electrolysis, IETE J. Res., 59 (2013) 280–288.
[24] B. M. Mohan, and A. Sinha, Mathematical models of the simplest Fuzzy PI/PD controllers with skewed input output fuzzy sets, ISA Trans., 47 (2008) 300–310.
[25] S. Bacha, D. Picault, B. Burger, I. Etxeberria-Otadui and J. Martins, Photovoltaics in microgrids: An overview of grid integration and energy management aspects, Ind. Electron. Mag. IEEE, 9(1) (2015) 33–46.
[26]. A. Lindiya, S. Palani, and A. Iyyappan, *Performance Comparison of Various Controllers for DC-DC Synchronous Buck Converter.* Procedia Engineering, 38(2012) 2679-2693.
[27] T. Guo, Z. Wang, X. Wang, S. Li, Q. Li, A simple control approach for buck converters with current-constrained technique, IEEE Transactions on Control Systems Technology, 27(1) (2017) 418-425.
[25] H. Moradi, G. Vossoughi, Robust control of the variable speed wind turbines in the presence of uncertainties: A comparison between H∞ and PID controllers, Energy, 90 (2015) 1508-1521.
[29] S. Abdelmalek, L. Barazane, A. Larabi, An advanced robust fault-tolerant tracking control for a doubly fed induction generator with actuator faults, Turkish Journal of Electrical Engineering & Computer Sciences, 25 (2017) 1346–1357.
[30] A. N. Vargas, L.P. Sampaio, L. Acho, L. Zhang, J.B. do Val, Optimal control of DC-DC buck converter via linear systems with inaccessible Markovian jumping modes, IEEE Transactions on Control Systems Technology, 24(5) (2015) 1820-1827.
[31] P. Song, C. Cui, Y. Bai, Robust output voltage regulation for DC–DC buck converters under load variations via sampled-data sensorless control, IEEE Access, 6 (2018) 10688-10698.
[32] J. Yang, B. Wu, S. Li, X. Yu, Design and qualitative robustness analysis of an DOBC approach for DC-DC buck converters with unmatched circuit parameter perturbations, IEEE Transactions on Circuits and Systems I: Regular Papers, 63(4) (2016) 551-560.
[33] J. Yang, H. Cui, S. Li, A. Zolotas, Optimized active disturbance rejection control for DC-DC buck converters with uncertainties using a reduced-order GPI observer, IEEE Transactions on Circuits and Systems I: Regular Papers, 65(2) (2017) 832-841.
[34] H. Du, C. Jiang, G. Wen, W. Zhu, Y. Cheng, Current sharing control for parallel DC–DC buck converters based on finite-time control technique, IEEE Transactions on Industrial Informatics, 15(4) (2018) 2186-2198.
[35] Y. Zheng, M. Ho, J. Guo, K.N. Leung, A single-inductor multiple-output auto-buck–boost DC–DC converter with tail-current control, IEEE Transactions on Power Electronics, 31(11) (2015) 7857-7875.
[36] K.E.L. Marcillo, D.A.P Guingla, W. Barra, R.L.P. De Medeiros, E.M. Rocha, D.A.V. Benavides, F.G. Nogueira, Interval robust controller to minimize oscillations effects caused by constant power load in a DC multi-converter buck-buck system, IEEE Access, 7 (2019) 26324-26342.

[37] A. Ardjal, A. Merabet, M. Bettayeb, R. Mansouri, L. Labib, Design and implementation of a fractional nonlinear synergetic controller for generator and grid converters of wind energy conversion system, Energy, 186 (2019) 115861.
[38] Z. Song, J. Hou, H. Hofmann, J. Li, M. Ouyang, Sliding-mode and Lyapunov function-based control for battery/supercapacitor hybrid energy storage system used in electric vehicles. Energy, 122 (2017) 601-612.
[39] H. Khayyam, A. Bab-Hadiashar, Adaptive intelligent energy management system of plug-in hybrid electric vehicle. Energy, 69 (2014) 319-335.
[40] S. Issaadi, W. Issaadi, A. Khireddine, New intelligent control strategy by robust neural network algorithm for real time detection of an optimized maximum power tracking control in photovoltaic systems, Energy, 187 (2019) 115881.
[41] N. Chettibi, A. Mellit, Intelligent control strategy for a grid connected PV/SOFC/BESS energy generation system, Energy, 147 (2018) 239-262.
[42] A. Bakdi, A. Kouadri, S. Mekhilef, A data-driven algorithm for online detection of component and system faults in modern wind turbines at different operating zones, Renewable and Sustainable Energy Reviews, 103 (2019) 546-555.
[43] A. Bakdi, W. Bounoua, S. Mekhilef, L.M. Halabi, Nonparametric Kullback-divergence-PCA for intelligent mismatch detection and power quality monitoring in grid-connected rooftop PV, Energy, 189 (2019) 116366.
[44] S. Abdelmalek , A. Dali, M. Bettayeb, A. Bakdi, A new effective robust nonlinear controller based on PSO for interleaved DC–DC boost converters for fuel cell voltage regulation. Soft Computing, 25(2020).
[45] Z. Xin-gang, Z. Ze-qi, X. Yi-min, M. Jin, Economic-environmental dispatch of microgrid based on improved quantum particle swarm optimization. Energy, 195 (2020) 117014.
[46] R. Eberhart, J. Kennedy, A new optimizer using particle swarm theory. In MHS'95. Proceedings of the Sixth International Symposium on Micro Machine and Human Science IEEE, (1995) 39-43.
[47] A. Dali, S. Abdelmalek, M. Bettayeb, A new combined observer-state feedback (COSF) controller of pwm buck converter, The International Conference on Electrical Sciences and Technologies in Maghreb (CISTEM), IEEE, 2018.
[48] S. Abdelmalek, A. Dali, M. Bettayeb, An improved observer-based integral state feedback (OISF) control strategy of flyback converter for photovoltaic systems, The International Conference on Electrical Sciences and Technologies in Maghreb (CISTEM), IEEE, 2018.
[49] A. Dali, A. Bouharchouche, S. Diaf, Parameter identification of photovoltaic cell/module using genetic algorithm (GA) and particle swarm optimization (PSO), The 3rd International Conference on Control, Engineering & Information Technology (CEIT), IEEE, 2015.
[50] S. Bendoukha, S. Abdelmalek, S. Abdelmalek, A new combined actuator fault estimation and accommodation for linear parameter varying system subject to simultaneous and multiple faults: an lmis approach, Soft Computing, 23 (2018) 10449–10462.
[51] S. Abdelmalek, L. Barazane, A. Larabi, M. Bettayeb, A novel scheme for current sensor faults diagnosis in the stator of a DFIG described by a TS fuzzy model, Measurement, 91 (2016) 680–691.
[52] S. Abdelmalek, L. Barazane, A. Larabi, H. Belmili, Contributions to diagnosis and fault tolerant control based on proportional integral observer: Application to a doubly-fed induction generator, The 4th IEEE International Conference on in Electrical Engineering (ICEE), (2015) 1–5.